IEEE Access
Multidisciplinary ⋮ Rapid Review ⋮ Open Access Journal

Received November 23, 2020, accepted November 29, 2020, date of publication December 9, 2020,
date of current version December 28, 2020.

Digital Object Identifier 10.1109/ACCESS.2020.3043656

Broadband Metasurface Antenna Using Hexagonal Loop-Shaped Unit Cells

WENZHANG ZHANG[1], CHAOYUN SONG[2], (Member, IEEE), RUI PEI[3], YI HUANG[1], (Senior Member, IEEE), AND JIAFENG ZHOU[1]

[1]Department of Electrical Engineering and Electronics, University of Liverpool, Liverpool L69 3GJ, U.K.
[2]School of Engineering and Physical Sciences, Heriot-Watt University, Edinburgh EH14 4AS, U.K.
[3]Department of Electrical and Electronics Engineering, Xi'an Jiaotong-Liverpool University, Suzhou 215123, China

Corresponding author: Jiafeng Zhou (jiafeng.zhou@liverpool.ac.uk)

This work was supported by the Royal Society International Exchanges Cost-share Programme under Grant IEC\NSFC\181364.

ABSTRACT A broadband metasurface antenna with a novel hexagonal loop-shaped unit cell structure is presented. A hexagonal loop element array is proposed as the main metasurface radiator, which is aperture-fed through a microstrip line and a coupling slot. The bandwidth can be broadened from two perspectives. On the one hand, the proposed hexagonal loop element is capable of generating broadband radiating bandwidth. On the other hand, due to the shape of the hexagonal loop structure, gaps between unit cells lead to a larger equivalent capacitance. This larger capacitance significantly pulls the fundamental resonant frequency downward, compared with conventional square structures, consequently leading to the broad bandwidth. In the design, the broadband performance is achieved by utilizing five TM modes at five resonant frequencies in the operational band from 4.65 GHz to 8.3 GHz. Apart from the fundamental TM_{01} mode, only TM_{12} modes were excited in different parts of the metasurface layer at different frequencies. This has ensured that the proposed antenna can maintain a stable radiation pattern in the desired band. The operation of the proposed antenna is analyzed in detail. The proposed hexagonal metasurface antenna with an overall size of $1.1\,\lambda_0 \times 1.1\,\lambda_0 \times 0.06\,\lambda_0$ can achieve 56.3% fractional bandwidth and a gain ranging from 7 to 11 dBi, which can be employed in satellite, radar, and wireless communication systems.

INDEX TERMS Broadband, characteristic mode analysis, hexagonal elements, metasurface.

I. INTRODUCTION

Over the last decades, wireless communication systems have witnessed rapid development. Novel designs of numerous microstrip antennas with advanced features of stabilized radiation patterns, compact size and wide impedance bandwidths are invented. Although merits in microstrip antennas such as low-profile and low-cost can be obtained, they still suffer from narrow operating bandwidths [1]–[5]. Various techniques have been investigated to improve the antenna bandwidth, employing aperture coupling, stacked patches, parasitic resonators, modified feeds, and reactive slot-loading [5]–[10], etc. Recently, a new perspective called metasurface (MTS) based antennas is proposed to improve the antenna bandwidth by means of manipulating electromagnetic waves [1]–[2]. As such, the impedance bandwidth and antenna gain can be significantly enhanced by placing an MTS right below or above the feeding aperture or microstrip patch [6]. In the literature, many MTS based antenna designs with both low-profile and broadband performance have been reported [3]–[12].

A dual-layer MTS antenna was investigated in [3], [4], providing good improvement of both impedance matching and antenna gain over a wide frequency range. Although two modes at different frequencies can be excited simultaneously, the total antenna profile was increased. Meanwhile, the gain is not stable over the operating frequencies. Instead of enlarging the size, in [5], broadband performance was fulfilled by cutting a slot at the center of the unit cell. It uses characteristic mode analysis to guide the MTS antenna design by exciting one MTS mode and one slot mode. The broadband performance is achieved by generating not only different mode types, but also the same type of mode with alternative modalities. While a lot of MTS antenna designs use a solid square patch as a unit cell, in [8], a non-periodic square-ring MTS antenna is proposed, which broadens the bandwidth by

The associate editor coordinating the review of this manuscript and approving it for publication was Mauro Fadda.

combining different resonance modes. It increases the number of modes on the MTS layer, and generates different resonance frequencies by tuning the square loop width. However, these designs have not considered the relationship between the shape of radiating elements and the bandwidth, which is potentially a direct method to broaden the bandwidth. As will be discussed in Section II and III, the potentially achieved bandwidth of the square unit cells, which are frequently seen in contemporary designs, might be narrower than the hexagonal ones. As such, it is a promising approach to engage hexagonal unit cells to construct MTS antennas.

In MTS antenna design, different unit cell geometries and layouts can potentially change its bandwidth and performance. It was found that a smooth transition on the structure edge to avoid sharp corners might bring smaller variation in the input impedance [22], resulting in the improvement in both bandwidth and impedance matching. The gap effect between unit cells and the structure layout also contribute to the bandwidth difference. For example, hexagonal elements as the radiating elements can potentially provide broadband performance [23]. The hexagonal loop element will further improve the impedance matching, implying an even broader bandwidth [24], [27].

In this paper, in order to achieve broadband performance, an MTS based antenna with hexagonal loop unit cells is proposed and analyzed. Compared with square unit cells, the hexagonal ones have shown capability to generate broader bandwidth. Meanwhile, the gaps between hexagonal loop elements can have larger capacitance values than that of conventional square ones, significantly pulling the fundamental resonant frequency downwards. As such, using hexagonal loop elements not only increases the bandwidth, but also decreases the size of the antenna. Additionally, by tuning the width of the loops, the hexagonal loop structure can be optimized to achieve a wider impedance bandwidth. The mode analysis techniques including basic antenna theories and characteristic mode analysis are applied to understand the working mechanism of the MTS antennas. Particularly, in the proposed MTS antenna with hexagonal loop unit cells of two different sizes, in total five modes will be excited over the operational band. Fed by a conventional aperture-coupled structure on the ground positioned right underneath the MTS layer, the proposed antenna can achieve a much broader bandwidth than conventional MTS antennas.

II. BANDWIDTH OF HEXAGONAL STRUCTURE

In MTS antennas, the choice of the element structure and the layout of the radiating elements determine the resonant frequencies and radiation bandwidth. The antenna performance can be improved by optimizing the shape of the radiating elements, as well as the gaps between neighboring elements. In this paper, the hexagon structure is chosen to design the proposed antenna to achieve a wider bandwidth compared with other antennas built based on traditional unit cells such as square or circular ones.

The reason that the hexagonal structure is a suitable option is mainly because unit cells incorporating tapered or rounded edges lead to the surface current flowing through smooth paths. The smooth transition on the edge of the radiating elements will cause smaller variation in the input impedance, defined as the impedance seen from the input port of the whole MTS antenna with the presence of the feeding structure. Such a difference will lead to the broad bandwidth performance and the impedance matching improvement [22]. Compared with conventionally designed square radiating elements [1]–[5], smoother transition brought by hexagonal unit cells will potentially enable the antenna to achieve wider bandwidth performance.

The characteristic mode analysis technique was employed to compare the bandwidth of hexagonal and square unit cells. With the aid of the characteristic mode analysis, the radiating bandwidth of a structure can be predicted without considering the feed. In modal significance, the radiating bandwidth of a mode is defined as the range of frequencies within which the power radiated by the mode is no less than one half the power (equivalent to, where λ_n is the eigenvalue of the generalized impedance matrix) [25]. To make a fair comparison, the tessellation of square elements and hexagonal elements with almost identical metallic areas are analyzed, as shown in Fig. 1. By evaluating the modal significance at the fundamental frequency, the hexagonal structure can achieve a wider radiating bandwidth (41%) than the square one (35%). Furthermore, as can be seen in Fig. 1(b) and Fig. 1(c), the characteristic current (depicted using red arrows) at the edge of the hexagonal element flows with a much smoother transition, compared with that of the square elements in which the current is flowing in straight lines. This is consistent with the explanations in the last paragraph. This smooth transition on the radiating element will consequently bring a gradual variation on the imaginary part of the input impedance [23], as depicted in Fig. 1(d). Such an appealing property brought by hexagonal elements will lead to a wider bandwidth.

However, not all radiating structures with a smooth transition on the edge are suitable choices, particularly when considering the influence on the bandwidth brought by gaps between neighboring elements. One representative example is the circular patch which has the smoothest structural transition. However, when the circular unit cells are used, gaps between composing elements cannot be kept constant. As demonstrated in [22], the bandwidth can be affected by changing impedance values. When considering potential influence between neighboring elements, the transition of gaps between neighboring circular elements is not constant, compared with that of hexagonal ones or square ones. The continuously variated distance in the gap will lead to different capacitance values, $C_1, C_2, \cdots, C_N$ as shown in Fig. 1(d). It will lead to drastic change on the imaginary part of the input impedance, degrading the matching and narrowing the bandwidth. It is also shown in Fig. 1(a) that the modal significance of circular radiating elements is the narrowest compared with hexagonal and square ones. In short, the hexagonal structure

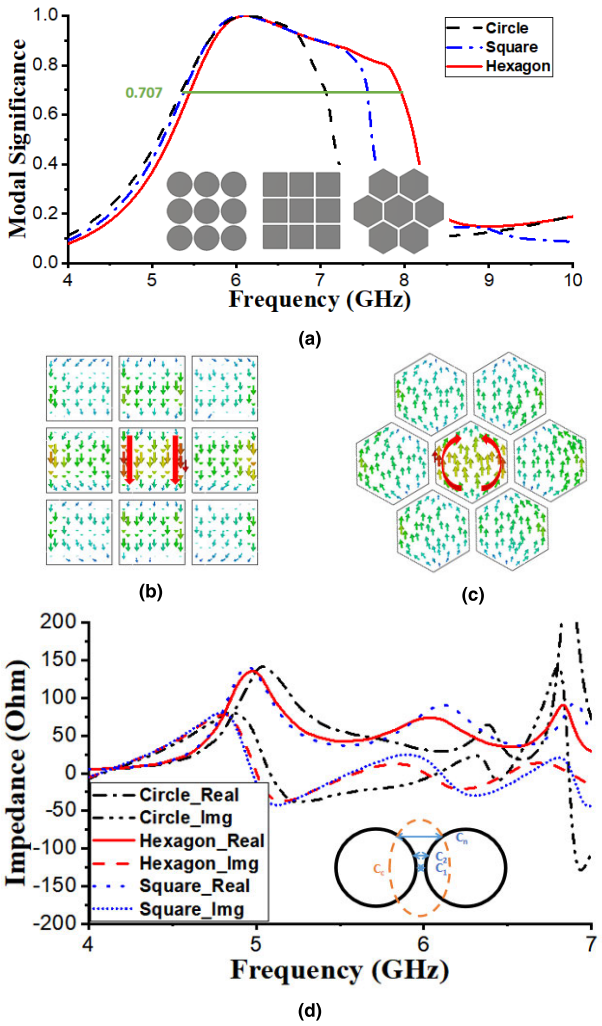

FIGURE 1. (a) The modal significance comparison between square, hexagonal and circular elements, and the characteristic current distributions on (b) square elements and (c) hexagonal elements. (d) The real and imaginary part of the impedance of various radiating elements (circle, square and hexagon).

has a wider bandwidth than the other two. Therefore, it is chosen as the radiating element.

III. MODE PREDICTION AND ANALYSIS OF METASURFACE ANTENNAS

A. POTENTIAL MODES IN A BASIC ANTENNA

To achieve broadband performance as analyzed above with the simplest and most compact settings, a basic MTS based antenna using hexagonal elements is designed. In this model, the basic MTS antenna consists of the MTS layer and the feeding layer. The geometry and detailed dimensions of the MTS layer and the feeding layer are shown in Fig. 2(a). These two layers are coupled through an aperture. A Rogers RO4003c substrate is used to connect these two parts together. The heights of two layers are 3.18 mm and 0.813 mm, respectively.

Potentially, both the TE and TM modes could be excited using MTS antennas. Nevertheless, as shown in Fig. 2(a), the

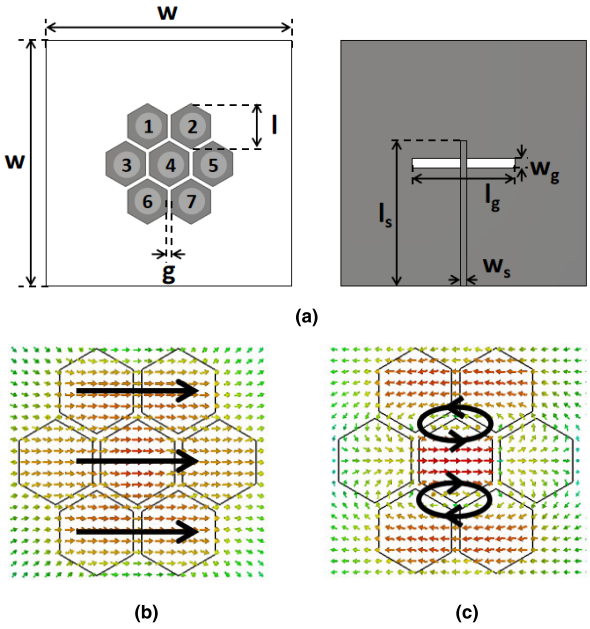

FIGURE 2. (a) Geometry of the basic MTS antenna using hexagonal radiating elements: MTS layer and feed layer (Dimensions: W = 60 mm, l = 10.5 mm, g = 1 mm, l_g = 25 mm, w_g = 2.4 mm, l_s = 35.5 mm, w_s = 1.55 mm). The magnetic field distributions at (b) the 1st frequency and (c) the 2nd frequency on the xoy plane.

basic antenna is fed by a microstrip line, along the y-axis. It is coupled to the MTS layer via the aperture on the ground plane. Consequently, there is no electric field vector parallel with the MTS surface generated by this feeding structure. In this sense, TE modes cannot be excited. On the contrary, TM modes can be easily excited, including the fundamental and higher TM modes. The fundamental TM mode is excited since the electromagnetic wave will be coupled from the microstrip line (along y-axis) to the center of the MTS via the center of the aperture. Fig. 2(b) verifies this prediction. The direction of the magnetic field on the MTS is along the x-axis.

Apart from the fundamental patch TM_{01} mode, it is also possible that higher TM_{xy} modes can be excited. The values of x and y are decided by different factors, which will be discussed as follows.

The value of x should be odd. As can be seen in Fig. 2(a), for hexagonal tessellation, the unit cells have to be placed in a staggered manner. Otherwise, non-tessellation or overlapping will occur if they are aligned in the conventional way as the case for square unit cells. Based on this staggered geometry, unit 1 and 2 are symmetric along the y-axis. In the area above the feed line, e.g. on unit 4 or on the gap between unit 1 and 2, the magnetic field must be parallel to the MTS surface along the x-axis. Therefore, the directions of magnetic field on unit 1 and 2 must be of the same direction. The same applies to unit 6 and 7 due to symmetry. Since the magnetic field must form complete loops, the number of loops along the x-axis direction must be an odd number. The directions of the magnetic field on unit 1 and unit 2 cannot be the same if the number of loops were an even number.

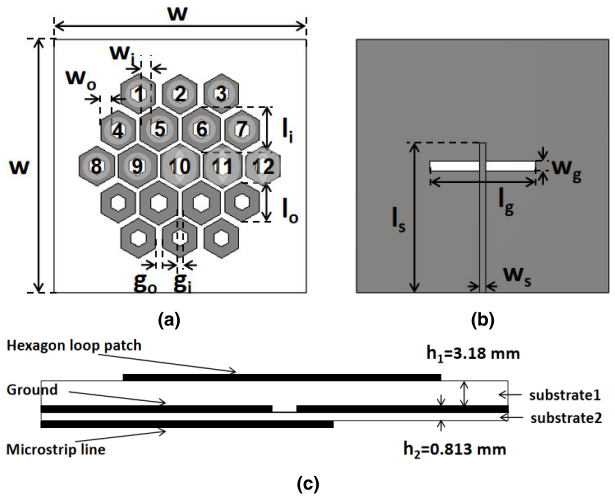

FIGURE 3. Geometry of the proposed MTS antenna using hexagonal loop unit cells. (a) Top view. (b) Bottom view. (c) Side view. ($W = 60$ mm, $l_i = 10.5$ mm, $l_o = 9.5$ mm, $w_i = 2.6$ mm, $w_o = 2.3$ mm, $g_i = 1$ mm, $g_o = 1.7$ mm, $l_g = 25$ mm, $w_g = 2.4$ mm, $l_s = 35.5$ mm, $w_s = 1.55$ mm).

Differently, the value of y is determined by the number of horizontal radiating gaps that are parallel to the aperture on the ground plane. Vertical gaps are not radiating because they are orthogonal to the aperture. For this reason, y is equal to 2 for lower modes since there are only two horizontal radiating gaps in this basic MTS antenna.

To verify the prediction, the magnetic field distributions at the 2nd resonant frequency are illustrated in Fig. 2(c). In each horizontal radiating gap, there will be one single closed magnetic field loop. Therefore, the MTS antenna operates at the TM_{12} mode. Higher modes are possible, but it will be beyond the frequency of interest.

B. MODE PREDICTION OF THE PROPOSED ANTENNA

To achieve a broader operating bandwidth, two changes are made to the fundamental antenna. Firstly, 12 extra hexagonal loop unit cells are placed outside of the basic MTS based antenna, as shown in Fig. 3. Secondly, hexagonal loop unit cells are used instead of hexagonal patch ones. This is because using loops can lower the resonant frequency of the MTS antenna [8]. The feeding structure is kept the same as the basic MTS antenna. In the proposed MTS antenna, there are in total 19 unit cells placed to form three concentric rings, namely the inner, the middle, and the outer ring with one, six, and 12 unit cells, respectively. Let UC-i denote the unit cell indexed as i as shown in Fig. 3(a). The notation of the unit cell set can be defined as {UC-i, i∈I}, where the set of I contains all the possible indices. Based on this, for the inner ring, it is UC-10. For the middle ring, it is {UC-i, i∈{5, 6, 9, 11, 14, 15}}. For the outer ring, it is {UC-i, i∈{1, 2, 3, 4, 7, 8, 12, 13, 16, 17, 18, 19}}. These three rings are seen in Fig. 3 (a). The unit cells in the inner and middle rings are of the same size. The size of unit cells in the outer ring is slightly smaller than those in the inner and middle rings, to be discussed in Section IV.A.

The same mode prediction approach demonstrated in Section III.A will be used to see only TM_{xy} modes can be excited. Specifically, the fundamental TM_{01} mode can still be excited since the microstrip line of the aperture coupled feeding part is along the y-axis. If x is not 0, it can only be an odd positive integer, as discussed in Section III.A.

As can be seen in Fig. 3, there are in total four horizontal radiating gaps in the proposed MTS antenna. Therefore, $y = 2$ or 4. Except for TM_{01}, two kinds of TM modes (TM_{x2} or TM_{x4}) can be possibly excited. The resonant frequencies of modes with $x > 1$ are too high for the operational band of interest. The resonant frequencies of modes with $y \geq 4$ are also very high. These high modes are not considered in this design. Therefore, only the TM_{12} mode can be excited.

However, the TM_{12} mode can be excited in different ways, i.e., at different radiating positions corresponding to different resonant frequencies. To better demonstrate this, those involved unit cells are divided into five rows. As shown in Fig.3 (a), the 1st row to the 5th row contain unit cells {UC-i, 1≤i≤3}, {UC-i, 4≤i≤7}, {UC-i, 8≤i≤12}, {UC-i, 13≤i≤16}, and {UC-i, 17≤i≤19}, respectively. Since the elements are symmetric, the electromagnetic field distribution on elements from the 1st to the 3rd rows will be symmetric to that from the 3rd to the 5th row. In the top half {UC-i, 1≤i≤12} in Fig. 3(a), closed magnetic field loops can be excited in two positions. One loop can be excited around the gaps between the 1st and the 2nd row. Another loop can be excited around the gaps between the 2nd and the 3rd row. In each case, the loop can involve different units. The resonant frequency of these modes is determined by the physical dimensions of the unit cells and the effective area of the units that generate the corresponding mode.

C. STUDY ON THE EXCITED MODES

To verify the prediction above, the operation of the antenna is evaluated by simulation. Five resonant frequencies can be observed in the simulation. The magnetic field distributions on the xoy planes are shown in Fig. 4. The magnetic field along the MTS layer is marked in black.

For the fundamental mode, the magnetic field distribution is similar to the patch antenna operating in the TM_{01} mode [1]. At the 2nd resonant frequency, in terms of the magnetic field, two closed magnetic loops can be observed on the radiation gap between unit cells {UC-i, i∈{4, 5, 6, 7, 9, 10, 11}} and {UC-i, i∈{9, 10, 11, 13, 14, 15, 16}}. The MTS antenna operates in an anti-phase TM_{12} mode.

As discussed in Section III.B, the MTS can operate in the TM_{12} mode in different ways. Another two resonant frequencies can be generated. As can be seen in Fig. 4(c) and Fig. 4(d) at the 3rd and 4th frequencies, respectively, the MTS operates in the anti-phase TM_{12} mode as well. However, these two modes differ from each other since the corresponding magnetic loops are in different areas. At the 3rd resonant frequency, two closed magnetic loops are mainly generated by unit cells {UC-i, 1≤i≤7}, and its symmetric area on the bottom half of the MTS surface. While at the 4th resonant frequency, the two loops are in the region of unit cells {UC-i, i∈{1, 2, 3, 5, 6}} and its symmetric region. Since the effective

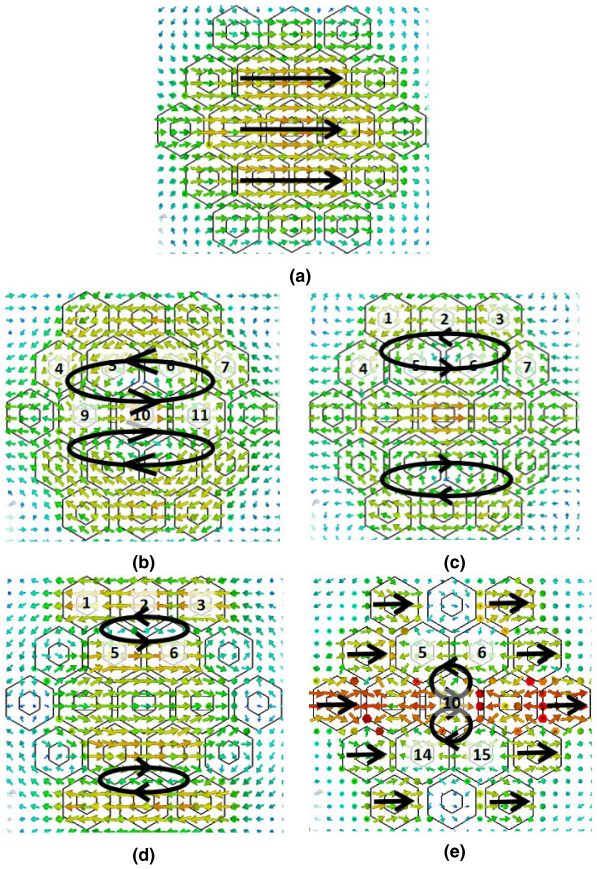

FIGURE 4. The magnetic field distributions on the xoy plane at (a) the 1st frequency, (b) the 2nd frequency, (c) the 3rd frequency, (d) the 4th frequency and (e) the 5th frequency.

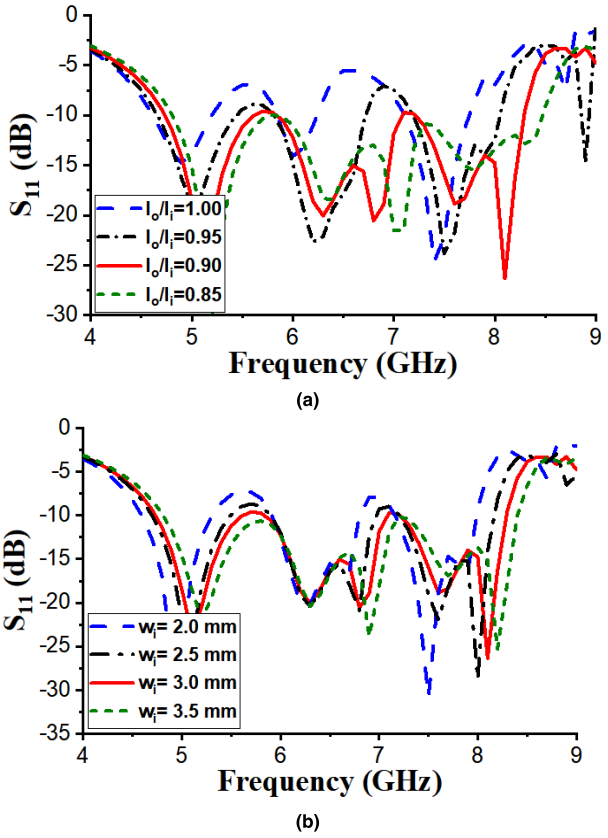

FIGURE 5. The S-parameter comparison of the antenna (a) with the same size of unit cells and the antenna with different sizes of unit cells on the MTS layer and (b) with different widths of unit cells.

area shaping the magnetic loop at the 3rd frequency is larger than that at the 4th one, the 3rd frequency is lower than the 4th frequency.

Due to that a similar number of unit cells are involved in the generation, the 2nd and 3rd frequencies would have been very close to each other. To separate the two frequencies, the units in the outer ring are slightly smaller than the units in the middle and inner rings. The 3rd frequency will be shifted higher, to improve the in-band performance of the antenna. This will be further discussed in section IV.

At the 5th resonant frequency, in Fig. 4(e), two closed magnetic loops are present around unit cells {UC-i, i∈{5, 6, 10}} and its symmetric region {UC-i, i∈{10, 14, 15}}. The magnetic field distribution pattern suggests that the MTS still mainly operates at the TM_{12} mode. However, since the operating frequency is relatively high, the surrounding unit cells {UC-i, i∈{1, 3, 4, 7, 8, 12, 13, 16, 17, 19}} also make contribution to the radiation. As a result, this radiation is influenced both by the anti-phase TM_{12} mode and parasitic element effect.

IV. PARAMETRIC STUDY

A. ELEMENT SIZE

It is interesting to investigate the effect of altering the dimensions of unit cells on different rings. It is noticed that each magnetic field loop is mainly generated by seven unit cells at the 2nd and the 3rd frequency, as shown in Fig. 4(b) and (c) respectively. The loops of the 2nd frequency are generated by unit cells on the middle and inner rings, while the loops of the 3rd frequency are on the middle and outer. Thus, a simple comparison is conducted by applying two different unit cell dimension settings: one is when all the unit cells are of the same size and the other is when the size of unit cells on the outer ring is different from the middle and inner rings. Such a variation will affect the anti-phase TM_{12} modes at the 2nd and the 3rd frequencies differently. The comparison result is shown in Fig. 5. It can be clearly seen that when unit cells are of the same size, the 2nd and the 3rd frequencies are very close to each other. When the ratio of the size of unit cells on the outer ring to that of others decreases, the difference between the 2nd frequency and 3rd frequency will increase. By changing the ratio of l_o/l_i (defined in Fig. 3) from 1 to 0.85, the difference of the two resonant frequencies is increased from 0 to 0.65 GHz. Therefore, the bandwidth can be increased, or the in-band performance can be improved by tuning the size of unit cells on the outer ring.

A further study is carried out to evaluate the effect of the width of the hexagonal loop. It has been studied in [8] that changing the width of a square loop will alter the resonant frequency of the loop. When the loop width w_i is decreased,

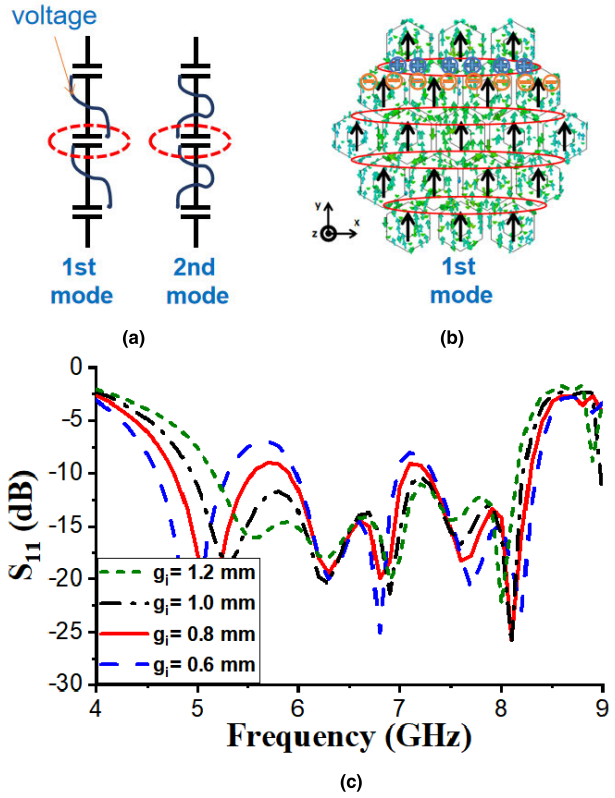

FIGURE 6. (a) The voltage difference, (b) the current distributions on the MTS layer at the 1st resonant frequency, and (c) the S-parameter comparison of the antenna with different gap widths between unit cells.

the resonant frequencies of all modes (the 1st frequency to the 5th frequency) will drop accordingly.

B. GAP EFFECT

When the gap width between each unit cell is decreased, the 1st frequency will decrease dramatically, while other frequencies remain almost stable. This is because the electric field distribution for the fundamental mode leads to significant voltage difference between adjacent unit cells [24]. The capacitance between unit cells significantly pulls the resonant frequency downward. In contrast to the fundamental mode, the resulted voltage differences are much mixed in other modes. It leads to insignificant variations on other resonant frequencies, as shown in Fig. 6(a).

At the fundamental frequency, due to the electric field distribution pattern at the TM_{01} mode, the corresponding current distributions on all units are polarized on the y-direction and in phase across the entire MTS layer. It will induce positive charges to accumulate on the bottom part of each row of unit cells and negative ones on the top part, and vice versa, as shown in Fig. 6(b).

As investigated in [24], due to the voltage difference between gaps at the fundamental frequency, increasing the capacitance between adjacent unit cells will significantly lower the resonant frequency. When considering the gap effect, hexagonal loop elements will form far greater

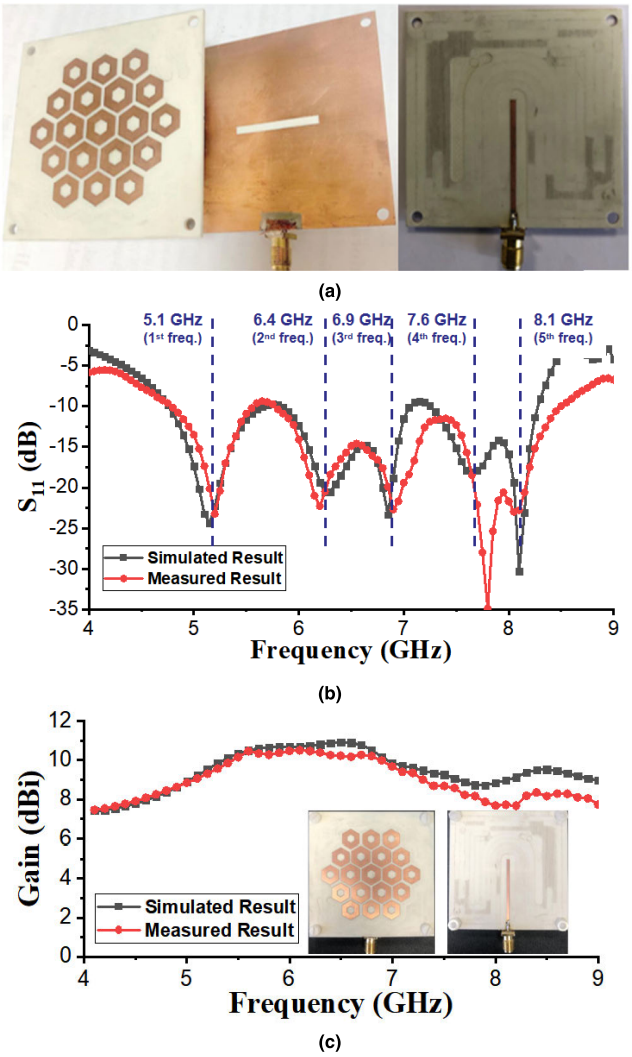

FIGURE 7. (a) Photographs of the fabricated antenna. Simulated and measured (b) S parameter and (c) gain of the proposed antenna.

equivalent capacitance compared with other types of elements, e.g., square ones [24].

Further verification of the relationship between the gap width and the frequency of the fundamental mode is shown in Fig. 6(c). When the gap width is decreased from 1.2 mm to 0.6 mm, the fundamental frequency was lowered by 16.7%, from 5.6 GHz to 4.8 GHz. Differently, because the electric field distributions are not as uniform in other modes, the gap width has much less effect on other resonant frequencies, as can be seen in Fig. 6(c).

In summary, decreasing the gap will significantly lower down the 1st frequency, while the resonant frequencies of other modes will be kept relatively constant. Taking this effect into consideration, the bandwidth of the antenna can be broadened by optimizing the gap width.

V. EXPERIMENTAL RESULTS

To validate the proposed design method, an MTS based antenna using hexagonal loop unit cells was prototyped and

TABLE 1. Performance comparison of broadband directional metasurface antennas.

Reference	Antenna Size (mm^3)	Center Frequency (GHz)	10 dB Impedance Bandwidth (%)	3 dB Gain Bandwidth (%)	Peak Gain (dBi)
[3]	1.1 λ_0 × 1.1 λ_0 × 0.09 λ_0	5.3 GHz	44%	45%	11.6
[4]	2.0 λ_0 × 2.0 λ_0 × 0.16 λ_0	6.5 GHz	55%	N/A (50%)	11.8
[5]	1.0 λ_0 × 1.0 λ_0 × 0.075 λ_0	5.6 GHz	25%	18%	10.3
[8]	1.1 λ_0 × 1.1 λ_0 × 0.06 λ_0	6.0 GHz	54%	32%	10.7
[26]	1.2 λ_0 × 1.2 λ_0 × 0.09 λ_0	7.0 GHz	67.3%	N/A (45%)	9.2
This work	1.2 λ_0 × 1.2 λ_0 × 0.09 λ_0	6.5 GHz	56%	48%	11.2

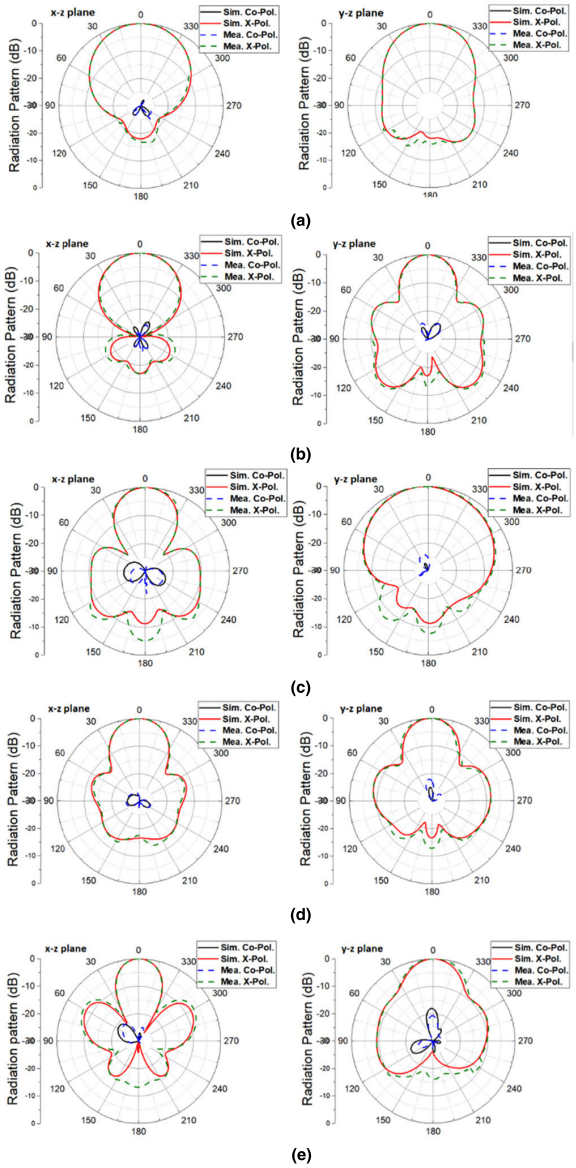

FIGURE 8. The simulated and measured radiation patterns of the proposed antenna at (a) 5.1 GHz, (b) 6.4 GHz, (c) 6.9 GHz, (d) 7.5 GHz and (e) 8.1 GHz.

measured, shown in Fig. 7(a). Dimensions of the antenna are illustrated in Fig. 3.

Fig. 7(b) presents a comparison between the simulated and measured S-parameters. The simulated bandwidth with reflection coefficient better than −10 dB is from 4.65 to 8.3 GHz while the measured bandwidth is from 4.7 to 8.5 GHz. The fractional bandwidth of the measure results is 57.6%, and the resonance frequencies are 5.1, 6.4, 6.9, 7.6, and 8.1 GHz, respectively. As a comparison, the simulated fractional bandwidth is 56.3%. The fabrication precision e.g., the tight connection between each layer and the fabrication error, will have greater effect at higher frequencies. As shown in Fig. 7(c), the simulated gain is from 7.7 to 11 dBi. By contrast, the measured gain is 7 to 11 dBi, which agrees with the simulated results very well.

The simulated and measured normalized radiation patterns at 5.1 GHz, 6.4 GHz, 6.9 GHz, 7.5 GHz and 8.1 GHz are shown in Fig. 8. They are in consistent agreement with the simulation. Due to the symmetrical feeding design, both the simulated and measured cross-polarization levels at boresight are below −30 dB in both the x-z and y-z planes across the operating frequency band. As can be seen, the proposed antenna has a very directional pattern at 5.1 GHz and 6.4 GHz. Meanwhile, the radiation patterns at 6.9 GHz and 7.5 GHz are with small side lobes. By contrast, relatively greater side lobes can be found in patterns at 8.1 GHz, which is mainly caused by the complexity of modes at higher frequencies as discussed in Section III. The discrepancy between the simulated and measured cross-polarization levels might be caused by the SMA connector used in the measurement, the fabrication errors, and the test environment variations. In general, consistent boresight radiation with a very low cross-polarization level has been achieved over the entire operating band.

The performance of the proposed antenna is compared with other broadband directional MTS antennas in Table 1. Particularly, designs in [3], [4] aim at improving the antenna performance by increasing the number of the MTS layers. The proposed hexagonal MTS antenna has achieved a similar fractional bandwidth (56%) with a single MTS layer compared with [4] (55%), and a broader bandwidth than [3] (44%). Compared with other relevant designs, e.g., [5], [8], the proposed hexagonal MTS antenna has achieved a broader 3 dB gain bandwidth (48% of the proposed one compared with 18% and 32% obtained by [5] and [8] respectively).

VI. CONCLUSION

A broadband MTS antenna using hexagonal loop unit cells has been proposed, analyzed and verified both theoretically and experimentally in this paper. The broadband performance

has been achieved for two main reasons. One is that a hexagonal loop element on its own has a broad radiation bandwidth than other conventional elements, such as square ones. The other is that the strong capacitance between hexagonal loop elements will lower the resonant frequency of the fundamental mode but keep other resonant frequencies relatively constant. The combination of these two factors has significantly broadened the operational bandwidth of the proposed antenna.

Due to the way the hexagonal elements were arranged in the metasurface layer, only TM_{12} modes at different positions have been excited in the operation band, in addition to the fundamental mode. Therefore, the proposed antenna can maintain a relatively stable radiation pattern. With a simple aperture-coupled feeding structure, the proposed antenna has achieved a fractional bandwidth of 56.3%, from 4.65 to 8.3 GHz, with a gain of 7 -11 dBi in the broad frequency band of interest. It has been proved that hexagonal elements are a suitable choice for broadband antenna design.

REFERENCES

[1] W. Liu, Z. N. Chen, and X. Qing, "Metamaterial-based low-profile broadband mushroom antenna," *IEEE Trans. Antennas Propag.*, vol. 62, no. 3, pp. 1165–1172, Mar. 2014.
[2] W. Liu, Z. N. Chen, and X. Qing, "Metamaterial-based low-profile broadband aperture-coupled grid-slotted patch antenna," *IEEE Trans. Antennas Propag.*, vol. 63, no. 7, pp. 3325–3329, Jul. 2015.
[3] Z.-Z. Yang, F. Liang, Y. Yi, D. Zhao, and B.-Z. Wang, "Metasurface-based wideband, low-profile, and high-gain antenna," *IET Microw., Antennas Propag.*, vol. 13, no. 4, pp. 436–441, Mar. 2019.
[4] H. Bai, G.-M. Wang, and T. Wu, "High-gain wideband metasurface antenna with low profile," *IEEE Access*, vol. 7, pp. 177266–177273, 2019.
[5] F. H. Lin and Z. N. Chen, "Low-profile wideband metasurface antennas using characteristic mode analysis," *IEEE Trans. Antennas Propag.*, vol. 65, no. 4, pp. 1706–1713, Apr. 2017.
[6] M. S. Alharbi, C. A. Balanis, and C. R. Birtcher, "Performance enhancement of square-ring antennas exploiting surface-wave metasurfaces," *IEEE Antennas Wireless Propag. Lett.*, vol. 18, no. 10, pp. 1991–1995, Oct. 2019.
[7] W. Sun, Y. Li, Z. Zhang, and P.-Y. Chen, "Low-profile and wideband microstrip antenna using quasi-periodic aperture and slot-to-CPW transition," *IEEE Trans. Antennas Propag.*, vol. 67, no. 1, pp. 632–637, Jan. 2019.
[8] D. Chen, W. Yang, W. Che, and Q. Xue, "Broadband stable-gain multiresonance antenna using nonperiodic square-ring metasurface," *IEEE Antennas Wireless Propag. Lett.*, vol. 18, no. 8, pp. 1537–1541, Aug. 2019.
[9] T. Li and Z. N. Chen, "A dual-band metasurface antenna using characteristic mode analysis," *IEEE Trans. Antennas Propag.*, vol. 66, no. 10, pp. 5620–5624, Oct. 2018.
[10] Q. Zheng, C. Guo, J. Ding, and G. A. E. Vandenbosch, "Dual-band metasurface-based CP low-profile patch antenna with parasitic elements," *IET Microw., Antennas Propag.*, vol. 13, no. 13, pp. 2360–2364, Oct. 2019.
[11] N. Hussain, M.-J. Jeong, A. Abbas, T.-J. Kim, and N. Kim, "A metasurface-based low-profile wideband circularly polarized patch antenna for 5G millimeter-wave systems," *IEEE Access*, vol. 8, pp. 22127–22135, 2020.
[12] J. Hu, G. Q. Luo, and Z.-C. Hao, "A wideband quad-polarization reconfigurable metasurface antenna," *IEEE Access*, vol. 6, pp. 6130–6137, 2018.
[13] C. Zhao and C.-F. Wang, "Characteristic mode design of wide band circularly polarized patch antenna consisting of H-shaped unit cells," *IEEE Access*, vol. 6, pp. 25292–25299, 2018.
[14] G. Feng, L. Chen, X. Xue, and X. Shi, "Broadband surface-wave antenna with a novel nonuniform tapered metasurface," *IEEE Antennas Wireless Propag. Lett.*, vol. 16, pp. 2902–2905, Sep. 2017.
[15] X. Yang, Y. Liu, and S.-X. Gong, "Design of a wideband omnidirectional antenna with characteristic mode analysis," *IEEE Antennas Wireless Propag. Lett.*, vol. 17, no. 6, pp. 993–997, Jun. 2018.
[16] T. Li and Z. N. Chen, "Metasurface-based shared-aperture 5G-band antenna using characteristic mode analysis," *IEEE Trans. Antennas Propag.*, vol. 66, no. 12, pp. 6742–6750, Dec. 2018.
[17] Y. M. Pan, P. F. Hu, X. Y. Zhang, and S. Y. Zheng, "A low-profile high-gain and wideband filtering antenna with metasurface," *IEEE Trans. Antennas Propag.*, vol. 64, no. 5, pp. 2010–2016, May 2016.
[18] W. Yang, S. Chen, Q. Xue, W. Che, G. Shen, and W. Feng, "Novel filtering method based on metasurface antenna and its application for wideband high-gain filtering antenna with low profile," *IEEE Trans. Antennas Propag.*, vol. 67, no. 3, pp. 1535–1544, Mar. 2019.
[19] N.-S. Nie, X.-S. Yang, Z. N. Chen, and B.-Z. Wang, "A low-profile wideband hybrid metasurface antenna array for 5G and WiFi systems," *IEEE Trans. Antennas Propag.*, vol. 68, no. 2, pp. 665–671, Feb. 2020.
[20] F. H. Lin, T. Li, and Z. N. Chen, "Recent progress in metasurface antennas using characteristic mode analysis," in *Proc. 13th Eur. Conf. Antennas Propag. (EuCAP)*, Krakow, Poland, 2019, pp. 1–5.
[21] M. Alibakhshi-Kenari, M. Naser-Moghadasi, R. A. Sadeghzadeh, B. S. Virdee, and E. Limiti, "Miniature CRLH-based ultra wideband antenna with gain enhancement for wireless communication applications," *ICT Exp.*, vol. 2, no. 2, pp. 75–79, Jun. 2016.
[22] D. E. Anagnostou, J. Papapolymerou, M. M. Tentzeris, and C. G. Christodoulou, "A printed log-periodic koch-dipole array (LPKDA)," *IEEE Antennas Wireless Propag. Lett.*, vol. 7, pp. 456–460, 2008.
[23] B. Munk, *Frequency Selective Surfaces: Theory and Design*. Hoboken, NJ, USA: Wiley, 2000.
[24] B. Majumder, K. Krishnamoorthy, J. Mukherjee, and K. P. Ray, "Compact broadband directive slot antenna loaded with cavities and single and double layers of metasurfaces," *IEEE Trans. Antennas Propag.*, vol. 64, no. 11, pp. 4595–4606, Nov. 2016.
[25] M. C. Fabrés, "Systematic design of antennas using the theory of characteristic modes," Ph.D. dissertation, Polytech. Univ. Valencia, Valencia, Spain, 2007, pp. 122–131.
[26] J. Wang, H. Wong, Z. Ji, and Y. Wu, "Broadband CPW-fed aperture coupled metasurface antenna," *IEEE Antennas Wireless Propag. Lett.*, vol. 18, no. 3, pp. 517–520, Mar. 2019.
[27] W. Zhang, C. Song, Y. Zhuang, Y. Huang, and J. Zhou, "Broadband hexagonal antenna based on metasurface using characteristic mode analysis," in *Proc. 13th Eur. Conf. Antennas Propag. (EuCAP)*, 2019, pp. 2–3.

WENZHANG ZHANG received the M.Sc. degree (Hons.) in electrical engineering and electronics from the University of Liverpool (UoL), Liverpool, U.K., in 2016, where she is currently pursuing the Ph.D. degree in wireless communications and RF engineering.

Her research interests include metasurface-based antenna and characteristic mode analysis.

CHAOYUN SONG (Member, IEEE) received the B.Eng., M.Sc., and Ph.D. degrees in electrical engineering and electronics from the University of Liverpool (UoL), Liverpool, U.K., in 2012, 2013, and 2017, respectively.

He is currently an Assistant Professor with the School of Engineering and Physical Sciences (EPS), Heriot-Watt University, Edinburgh, U.K. He was a Postdoctoral Research Associate with UoL, from 2017 to 2020. He has published more than 70 papers (including 30 IEEE transactions) in peer-reviewed journals and conference proceedings. He holds two U.S. patents and two U.K. patents. His current research interests include wireless energy harvesting and wireless power transfer technologies, antennas and microwave circuits using novel materials, dielectric material and ionic liquids in RF applications, metamaterials and meta-surfaces in RF, energy harvesting, and sensing technologies.

Dr. Song was a recipient of many international awards, such as the BAE Systems Chairman's Award, in 2017, for the innovation of next generation global navigation satellite system antennas. In 2018, he received the highly-commended award from the prestigious IET Innovation Awards over three categories–"Energy and Power," "Emerging Technologies," and "Young Innovators." He has been a regular reviewer of more than 25 international journals, including *Nature Communications*, *Applied Physics Letters*, *Nano Energy*, and seven IEEE transactions, and a Guest Editor of *Wireless Communications and Mobile Computing*.

RUI PEI received the joint B.Eng. degree (Hons.) from Xi'an Jiaotong-Liverpool University and the University of Liverpool, in 2015, and the M.Sc. degree (Hons.) from the University of Edinburg, in 2016. He is currently pursuing the Ph.D. degree with the University of Liverpool.

His research interests include antenna design, wearable antennas, metamaterials, specific absorption rate, and body area networks.

YI HUANG (Senior Member, IEEE) received the B.Sc. degree in physics from Wuhan University, China, in 1984, the M.Sc. (Eng.) degree in microwave engineering from NRIET, Nanjing, China, in 1987, and the D.Phil. degree in communications from the University of Oxford, U.K., in 1994. He has been conducting research in the areas of wireless communications, applied electromagnetics, radar, and antennas, since 1987. His experience includes three years spent with NRIET, China, as a Radar Engineer, and various periods with the Universities of Birmingham, Oxford, and Essex, U.K., as a member of research staff. He worked as a Research Fellow at British Telecom Labs, in 1994, and then joined the Department of Electrical Engineering and Electronics, University of Liverpool, U.K., as a Faculty in 1995, where he is currently a Full Professor in Wireless Engineering, the Head of High Frequency Engineering Group, and the Deputy Head of Department. He has published over 350 refereed papers in leading international journals and conference proceedings, and authored *Antennas: from Theory to Practice* (John Wiley, 2008) and *Reverberation Chambers: Theory and Applications to EMC and Antenna Measurements* (John Wiley, 2016). He has received many research grants from research councils, government agencies, charity, EU, and industry, acted as a consultant to various companies, and served on a number of national and international technical committees, and has been an editor, associate editor, and guest editor of five international journals. He has been a keynote/invited speaker and organizer of many conferences and workshops (e.g., WiCom 2006 and 2010, IEEE iWAT2010, LAPC2012, and EuCAP2018). He is currently the Editor-in-Chief of *Wireless Engineering and Technology*, an Associate Editor of IEEE Antennas and Wireless Propagation Letters, U.K., an Ireland Representative to European Association of Antenna and Propagation (EurAAP), a Fellow of IET, and a Senior Fellow of HEA.

JIAFENG ZHOU received the B.Sc. degree in radio physics from Nanjing University, Nanjing, China, in 1997, and the Ph.D. degree from the University of Birmingham, Birmingham, U.K., in 2004. His doctoral research concerned high-temperature superconductor microwave filters.

In July 1997, he was with the National Meteorological Satellite Centre of China, Beijing, China, for two and a half years, where he was involved with the development of communication systems for Chinese geostationary meteorological satellites. From August 2004 to April 2006, he was a Research Fellow with the University of Birmingham, where his research concerned phased arrays for reflector observing systems. Then, he moved to the Department of Electronic and Electrical Engineering, University of Bristol, Bristol, U.K., until August 2013, where his research was on the development of highly efficient and linear amplifiers. He is currently with the Department of Electrical Engineering and Electronics, University of Liverpool, Liverpool, U.K. His current research interests include microwave and radio frequency components and devices, metamaterials, electromagnetic energy harvesting, and wireless power transfer.